



Published in final edited form as:

Ultrasound Med Biol. 2010 March ; 36(3): 419–429. doi:10.1016/j.ultrasmedbio.2009.11.009.

CAVITATION PROPERTIES OF BLOCK COPOLYMER STABILIZED PHASE-SHIFT NANOEMULSIONS USED AS DRUG CARRIERS

NATALYA RAPOPORT^{1,*}, DOUGLAS A. CHRISTENSEN^{1,2}, ANNE M. KENNEDY³, and KWEONHO NAM¹

¹Department of Bioengineering, University of Utah, Salt Lake City, UT, USA

²Department of Electrical and Computer Engineering, University of Utah, Salt Lake City, UT, USA

³Department of Clinical Radiology, School of Medicine, University of Utah, Salt Lake City, UT, USA

Abstract

Cavitation properties of block copolymer stabilized perfluoropentane nanoemulsions have been investigated. The nanoemulsions were stabilized by two biodegradable amphiphilic block copolymers differing in the structure of the hydrophobic block, poly(ethylene oxide)-co-poly(L-lactide) (PEG-PLLA) and poly(ethylene oxide)-co-polycaprolactone (PEG-PCL). Cavitation parameters were measured in liquid emulsions and gels as a function of ultrasound pressure for unfocused or focused 1-MHz ultrasound. Acoustic droplet vaporization preceded generation of acoustic cavitation in liquid matrices and gels. Both stable and inertial cavitation was observed for focused ultrasound while only stable cavitation was observed for unfocused ultrasound.

Keywords

Nanoemulsions; Microbubbles; Acoustic droplet vaporization; Cavitation

INTRODUCTION

Severe side effects of current tumor chemotherapy are caused by drug interaction with healthy tissues. To solve systemic toxicity problems, various drug delivery modalities have been suggested that are commonly based on drug encapsulation in nanocarriers such as liposomes, polymeric micelles, and hollow nanocontainers. These drug nanocarriers are targeted to tumors either passively or actively. Tumor targeting of nanocarriers is based on the enhanced permeability of defective tumor microvasculature that allows extravasation of drug-loaded nanoparticles through large inter-endothelial gaps; the inter-endothelial gaps in tumors may be 750 nm or even larger (Campbell 2006, Hobbs, Monsky 1998). In addition, poor lymphatic drainage of tumors provides long retention of extravasated particles in tumor tissues. This effect is called enhanced permeability and retention, or EPR (Iyer, Khaled 2006). In contrast to tumors, blood vessels in normal tissues have tight inter-endothelial junctions (cutoff size of about 7 nm) that do not allow extravasation of nanoparticles (Campbell 2006). An elevated interstitial pressure within tumors is a potential barrier to intratumoral drug delivery, but an elevated pressure is mostly observed in internal necrotic area while actively growing tumor margins experience substantially lower pressures (Campbell 2006).

*Address correspondence to: Dr. Natalya Rapoport, 72 South Central Campus Drive, Room 2646, Department of Bioengineering, University of Utah, Salt Lake City, UT 84112, USA. Natasha.rapoport@utah.edu.

The effective tumor accumulation of nanoparticles *via* the EPR effect requires sufficient particle residence time in circulation; to provide for this, nanoparticles are commonly coated with poly(ethylene oxide) chains that suppress blood protein adsorption and prevent particle recognition by the cells of the reticuloendothelial system.

An effective approach to tumor targeting of drug nanocarriers consists of developing stimuli-responsive nanoparticles that release their drug load only in response to tumor-specific or tumor-directed environmental or physical stimuli such as pH, hyperthermia, light, or ultrasound. Using ultrasound as a drug delivery stimulus is especially attractive because it allows combining costeffective ultrasound imaging with ultrasound-mediated therapy. Tumor sonication with millimeter precision is feasible; with a proper modeling that accounts for the effects of attenuation and aberration along the ultrasonic beam path, ultrasound may be directed toward deeply located body sites in precise energy deposition patterns. Sonication may be performed non-invasively or minimally invasively through intraluminal, laparoscopic or percutaneous means.

Several groups concentrated their efforts on developing ultrasound-responsive drug delivery systems (Ferrara, Burden 2009, Hynynen 2008, Unger, Porter 2004). Ferrara's group has recently reported development of ultrasound-responsive stable liposomes that manifested prolonged circulation time and effective tumor targeting; functionalizing these particles with positron emission tomography (PET) and optical markers enabled multimodality imaging of their biodistribution. Heating triggered phase transition in the phospholipid membrane and released the drug in the target region. These systems can be excellent for delivery of hydrophilic drugs that can be encapsulated with a high degree of loading in the inner liposomal compartments.

During the last decade, developing microbubble-based drug delivery systems has attracted attention (Ferrara, Pollard 2007, Hernot and Klibanov 2008, Unger, Porter 2004, Wheatley, Forsberg 2006). For many decades, microbubbles have been used as contrast agents in ultrasound imaging. It would be attractive to impart drug delivery properties to the phospholipid- or albumin-coated microbubbles already approved by the U. S. Food and Drug Administration as ultrasound contrast agents. However, these systems have two inherent problems. The ideal tumor-targeted microbubble-based drug carrier should satisfy the following criteria: (i) stability in circulation; (ii) prolonged circulation time to allow for effective accumulation in the targeted tissue; (iii) size that allows extravasation through tumor microvasculature (hundred nanometers); and (iv) efficient release of drug locally in tumor tissue in response to an external stimulus such as tumor-directed ultrasound. The cutoff size of inter-endothelial gaps in tumor microvasculature depends on the tumor type and ranges from 300 nm to 780 nm (Campbell 2006, Hobbs, Monsky 1998). For microbubbles that are used as ultrasound contrast agents, a very short circulation time (minutes) and several micron size do not allow effective extravasation into tumor tissue, an essential prerequisite for effective drug targeting when utilizing the EPR of the tumor..

One way to solve this problem consists in developing nano-sized microbubble precursors that would effectively accumulate in tumor tissue *via* the EPR effect and then convert into microbubbles *in situ* under the action of tumor-directed ultrasound. With this in mind, we have recently developed novel, stable, drug-loaded perfluorocarbon nanoemulsions, the walls of which are formed by amphiphilic block copolymers (Gao, Kennedy 2008, Rapoport, Gao 2007). These systems differ in a number of ways from those currently used as ultrasound contrast agents: (i) the bubbles are produced *in situ* upon injection of specially designed nanoemulsions; (ii) the nanodroplets have walls produced by biodegradable diblock copolymers that provides for high *in vivo* stability and allows accumulation in the tumor volume *via* extravasation through defective tumor microvasculature (i.e. *via* passive targeting)

(Rapoport, Kennedy 2009); (iii) drugs (DOX and PTX) are tightly retained by the nanodroplets (Rapoport, Kennedy 2009); (iv) upon tumor accumulation of nanodroplets, localized ultrasonic irradiation of the tumor by therapeutic ultrasound results in localized drug release and effective intracellular drug uptake leading to effective tumor regression (Gao, Kennedy 2008, Rapoport, Gao 2007, Rapoport, Kennedy 2009); and (v) upon droplet-to-bubble transition, tumor-accumulated bubbles produce long-lasting ultrasonic imaging contrast (Gao, Kennedy 2008, Rapoport, Gao 2007, Rapoport, Kennedy 2009, Rapoport, Efros 2009).

Vaporization properties of these nanodroplets were discussed in ref. (Rapoport, Efros 2009). Their therapeutic properties were reported in detail in ref. (Rapoport, Kennedy 2009). The results obtained in these studies are briefly summarized below. Three factors that induced droplet-to-bubble transition inside nanodroplets were identified: thermal (heating), mechanical (injection through a fine-gauge needle), and acoustic (thermal and/or mechanical). Of the factors listed, ultrasound was the most powerful. Low efficacy of heating is associated with Laplace pressure that is developed inside spherical droplets:

$$\Delta P = P_{\text{inside}} - P_{\text{outside}} = \frac{2\sigma}{r} \quad (1)$$

where P_{inside} is the pressure inside a droplet, P_{outside} is the pressure outside a droplet, σ is the surface tension, and r is droplet radius. PFP has a boiling temperature of 29 °C at atmospheric pressure, which is close to room temperature, however, Laplace pressure inside a droplet may significantly increase the PFP boiling temperature. This effect is inversely proportional to droplet size (Rapoport, Kennedy 2009, Rapoport, Efros 2009). According to eq. 1, droplets possess a distribution of boiling temperatures corresponding to their size distribution. Another significant factor that controls PFP boiling temperature is the surface tension σ at the droplet/environment interface. This parameter depends on the type of droplet stabilizing copolymer. The surface tension at the PFP/water interface for “naked” (i.e. not surfactant coated) PFP droplets is 56 ± 1 mN/m (Clasohm, Vakarelski 2007). This is the upper limit of a possible surface tension which is expected to be decreased when the droplet is coated with a surface active copolymer.

Vaporization temperatures of droplets of different sizes may be estimated using the Antoine equation for temperature dependence of vapor pressure, with the coefficients for PFP given in ref. (Barber and Cady 1956):

$$\log_{10} P = A - \left(\frac{B}{T+C} \right) \quad (2)$$

where T is absolute temperature and A , B , and C are constants. The dependence of a PFP vaporization temperature on droplet size was estimated for two values of surface tension, $\sigma = 30$ mN/m and $\sigma = 50$ mN/m (Rapoport, Kennedy 2009). This estimation showed that at physiological temperature, the droplets with the diameter below 4 μm (for $\sigma = 30$ mN/m) or 6.4 μm (for $\sigma = 50$ mN/m) will remain in a liquid state, while larger droplets will vaporize to form microbubbles. This estimation suggests that upon systemic injection of our formulations, the nanodroplets are expected to remain in a liquid state and therefore maintain their nano-scale size, which is important for their extravasation and accumulation in tumor tissue. The accumulation of nanodroplets in tumor tissue after systemic injection was monitored and confirmed by ultrasound imaging for breast (Rapoport, Gao 2007) and pancreatic tumor (Rapoport, Kennedy 2009).

Partial droplet-to-bubble transition in the nanodroplet population proceeded at room temperature upon droplet injection through small diameter needles (Rapoport, Efros 2009). This effect was of purely mechanical origin and may be caused by either shear stresses developed on droplet surfaces or pressure gradients in the injected stream. This effect deserves further investigation and may be clinically beneficial, because microbubbles in circulation may increase permeability of tumor capillaries and enhance nanodroplet extravasation under the action of tumor-directed therapeutic ultrasound (Bekeredjian, Chen 2003, Chappell, Klibanov 2005, Kinoshita, McDannold 2006, Miller and Gies 1998, Skyba, Price 1998, Stieger, Caskey 2007). However, generation and size of microbubbles in circulation should be carefully controlled to avoid embolization.

The ultrasound-induced droplet-to-bubble transition (acoustic droplet vaporization, ADV) and acoustic cavitation of formed bubbles are the most important therapeutically related processes. ADV of albumin-stabilized PFP nanodroplets was investigated in a series of publications (Kripfgans, Fabiilli 2004, Kripfgans, Fowlkes 2000, Lo, Kripfgans 2007). For block copolymer stabilized PFP nanodroplets used in our studies, the ADV effects were reported in refs. (Rapoport, Kennedy 2009, Rapoport, Efros 2009). It was found that ultrasound-induced formation of microbubbles in gel matrices was substantially hampered in comparison to liquid emulsions (Rapoport, Efros 2009). It was hypothesized that this effect was due to higher resistance to the expansion of the droplet wall during droplet-to-bubble transition. An alternative mechanism may be related to decreased coalescence of microbubbles formed by ADV. Coalescence increases bubble sizes and may lead to the irreversible formation of stable bubbles. Decreased diffusion in viscous matrices may restrict or preclude bubble coalescence. It was shown that the formation of the stable bubbles inside gel matrices was catalyzed by pre-existing large bubbles, especially at low ultrasound frequencies (Rapoport, Kennedy 2009, Rapoport, Efros 2009).

In contrast to secondary microbubbles formed via bubble coalescence, the size of primary microbubbles formed via ADV from nanodroplets of up to 750 nm diameter would be less than four microns (see Discussion), which corresponds to boiling temperatures above physiological temperatures (Rapoport, Kennedy 2009, Rapoport, Efros 2009). For these bubbles, the ADV effect is reversible and these bubbles condense back into liquid droplets upon turning ultrasound off or during inter-pulse intervals of pulsed ultrasound. Primary microbubbles are expected to undergo cavitation under the action of therapeutic ultrasound in the low megahertz frequency range. Stable cavitation of microbubbles was implicated as the main mechanism of the enhanced gene or drug delivery (Greenleaf, Bolander 1998, Hernot and Klibanov 2008, Mehier-Humbert, Yan 2007, Rapoport, Gao 2007, Suzuki, Takizawa 2007). In our research, we observed effective regression of breast, ovarian, and pancreatic tumors treated by paclitaxel-loaded PFP nanoemulsions combined with tumor-directed 1-MHz or 3-MHz therapeutic ultrasound (Rapoport, Gao 2007, Rapoport, Kennedy 2009). It was postulated that ultrasound triggered droplet-to-bubble transition and induced release of the encapsulated drug from the bubble coating (Rapoport, Kennedy 2009). Efficient drug release was presumably related to either stable or inertial acoustic cavitation of microbubbles inside tumor tissue. Many details of the mechanism of the droplet-to-bubble transition are still unclear. In this work, we have studied acoustic cavitation of copolymer stabilized PFP nanodroplets in the range of ultrasound parameters that were used in vivo (Rapoport, Gao 2007, Rapoport, Kennedy 2009). Nanodroplets were either placed in liquid emulsions or inserted into 0.6% agarose gel phantoms that mimicked tumor tissue.

MATERIALS AND METHODS

Block copolymers

Block copolymers used in this study were from Polymer Source Inc. (Montreal, Quebec, Canada). The poly(ethylene oxide)-co-poly(L-lactide) (PEG-PLLA) copolymer had a total molecular weight of 9,700 Da; the molecular weights of a hydrophilic PEG block and a hydrophobic PLLA block were 5,000 Da and 4,700 Da respectively. The number of the monomer units in the corresponding blocks was 113.6 and 54.7. The poly(ethylene oxide)-copolycaprolactone (PEG-PCL) copolymer had a total molecular weight of 4,600 Da; the molecular weights of a PEG block and PCL block were 2000 Da and 2600 Da respectively. The number of monomer units in the corresponding blocks was 45.5 and 22.8.

Micellar solutions

Micellar solutions of the PEG-PLLA and PEG-PCL block copolymers were prepared by a solvent exchange technique as described in detail previously (Rapoport, Gao 2007).

Nanoemulsions

Perfluoropentane (PFP) nanoemulsions were prepared as follows: 1% vol. perfluoropentane (PFP) (Apollo Scientific Stockport, Cheshire, UK) was added to a PEG-PLLA or PEG-PCL micellar solution and samples were sonicated in ice-cold water by 20-kHz ultrasound (VCX500, Sonics & materials Inc., Newtown, CT, USA) until all PFP was transferred into an emulsion.

Nanodroplet introduction into gels

The nanodroplets were mixed with 0.2% or 0.6% agarose solution in phosphate buffered saline (PBS) before gel formation. The liquid mixture was placed in a Samco transfer pipette (5-mm inner diameter, 0.3-mm wall thickness) (Fisher Scientific, Pittsburg, PA, USA) and cooled down to room temperature for gel formation.

Particle size distribution

Size distribution of nanoparticles was measured by dynamic light scattering at a scattering angle of 165° using Delsa Nano S instrument (Beckman Coulter, Osaka, Japan) equipped with a 658-nm laser and a temperature controller. Particle size distribution was analyzed using the non-negative least squares (NNLS) method (software was provided by the manufacturer).

The instrument allows measurement of particle sizes from 0.6 nm to 7 µm; microparticles larger than 7 µm cannot be measured accurately. Optical monitoring of the samples using an inverted microscope and hemacytometer (model 3200, Hauser Scientific, Horsham, PA, USA) showed no microdroplets larger than 7 µm. The hemacytometer was used for measuring the mean concentration of microdroplets.

Sonication

Unfocused 1-MHz ultrasound was generated by an Omnisound 3000 instrument (Accelerated Care Plus Inc, Sparks, NV, USA) equipped with a 1-cm² piezoceramic crystal and 5-cm² probe head. Focused 1MHz ultrasound was generated by a high intensity focused ultrasound (HIFU) transducer (H-101, Sonic Concepts, Bothell, WA, USA) with an active diameter of 64 mm and focal length of 63 mm. The -3 dB lateral and axial pressure profiles were 1.2 and 10 mm respectively. Transducer was driven by an arbitrary waveform generator (33120A, Agilent, Santa Clara, CA, USA) connected to a 50-dB RF power amplifier (Model 240L, Electronics Navigation Industries, Rochester, NY, USA). The nanodroplet formulation, drawn into a Samco polyethylene transfer pipette (5-mm inner diameter, 0.3-mm wall thickness) (Fisher

Scientific Pittsburg, PA, USA) was positioned either at a distance of 0.5 cm from the unfocusing transducer or at the focal zone of the focusing transducer (See the scheme and the photograph, Figure 1). The focal point of a HIFU transducer was detected using an xyz-positioner and hydrophone. The arrangement was housed in an open glass tank containing filtered distilled degassed water maintained at room temperature or 37 °C using a temperature controller (Polystat, Cole-Parmer, Vernon Hills, IL, USA). To minimize possible standing wave formation, an absorbing rubber liner was mounted opposite the transducer.

Ninety kilohertz ultrasound was generated in the SC-100 ultrasound bath (Sonicor Instrument Co., Copiague, NY, USA).

Monitoring acoustic droplet vaporization by visual observation and ultrasound imaging

The ultrasound-induced formation of microbubbles from nanodroplets was monitored at room temperature visually and by ultrasound imaging, based on a higher echogenicity of bubbles compared to droplets (Kripfgans, Fowlkes 2000, Lo, Kripfgans 2007); a 7.5-MHz linear array scanner (Scanner 250, Pie Medical, Maastricht, The Netherlands) was used for ultrasound imaging with 14 frames per second scan rate (see scheme of Figure 1A). The samples in Samco transfer pipettes (5-mm inner diameter, 0.3-mm wall thickness, 2 mm diameter of the narrow bottom part, see Figure 1B) were allowed to precipitate overnight to the bottom of the transfer pipette. The samples were then sonicated by 1-MHz ultrasound starting with the lowest pressure of 0.14 MPa generated by the Omnisound 3000 instrument at the site of the sample. The pressure was increased stepwise and the formation of the upward directed bubble stream was monitored. The lowest pressure that induced bubble stream formation was considered corresponding to or being above the ADV threshold for the formation of primary bubbles. Due to a stepwise nature of the pressure increase, we can only state that the ADV threshold for a particular sample was located in the interval between the highest pressure that did not induce bubble formation and the next step pressure that induced vaporization.

By assuming a 125-fold density difference between the PFP in the liquid and gaseous phases, we estimated that the density of a droplet will be equal to the water density when the degree of vaporization inside an individual droplet equals 40%. At a higher degree of vaporization, droplets will rise in water. At each ultrasound power, the ultrasound was turned off to monitor if bubbles precipitated to the bottom of the test tube due to reversibility of vaporization or were rising to the sample surface due to the irreversible formation of stable bubbles. The resolution of the ultrasound images was lower than 200 μm , thus bubbles observed by imaging (Figure 2) were most probably secondary bubbles formed *via* coalescence of primary bubbles. Still, visual observation of the initial bubble stream formation and ultrasound imaging produced close results on the ADV thresholds suggesting that ADV was a limiting step for bubble coalescence (i.e. bubble coalescence occurred faster than droplet vaporization). The results were reproducible in parallel runs.

Cavitation activity

These measurements were performed with the samples placed in the transfer pipettes. Before placement into the transfer pipette, the samples were carefully pumped in and out in order to lift the precipitated droplet population and mix the sample. Cavitation activity was assessed by measuring harmonic, subharmonic, and broadband noise amplitudes in a portion of the scattered beam. In order to detect the acoustic emissions from cavitation, a needle hydrophone (HNR-0500, Onda, Sunnyvale, CA, USA) with a 20-dB preamplifier (AH-1100, Onda, Sunnyvale, CA, USA) was mounted at a 90° angle to the transducer (See Figure 1); the vertical position of the hydrophone corresponded to the center of the sample holder. The radiofrequency (RF) signals were digitized with a sampling frequency of 500 MHz with an oscilloscope (TDS 3012B, Tektronix, Beaverton, OR, USA). For ten seconds, a total of 15 recordings of time-

domain RF signals emitted from the droplets samples were acquired for each ultrasound pressure level and stored on a laptop computer for further analysis. The temporal waveform was gated with a 40 μ s Hamming window and the fast Fourier transform (FFT) was computed to determine frequency content. Broadband noise was quantified as the root-mean-square (RMS) over a selected combination of frequency bands (0.6–0.9 MHz, 1.1–1.4 MHz, 1.6–1.9 MHz, 2.1–2.4 MHz, and 2.6–2.9 MHz for 1-MHz ultrasound) to isolate the broadband emission from the fundamental, harmonic, and ultraharmonic frequencies. The amplitude of a subharmonic component was taken from the peak in the FFT spectrum at the half of the fundamental frequency. The relative level (RL) of the broadband noise and the harmonic components were each calculated according to the following equation:

$$RL = \frac{L_S - L_B}{L_B}, \quad (2)$$

where the L_S and L_B indicate the amplitude levels from a sample and from water in the tank, respectively; the amplitude for water was taken at the lowest insonation pressure as a noncavitating baseline. A total of 75 FFT spectra from five measurements at each insonation pressure were averaged. The pressure levels presented in the paper are peak rarefactional pressures. All data were processed using Matlab software. The cavitation threshold was defined as the acoustic pressure at which the difference between the corresponding signal amplitudes for the sample and control (which is PBS or pure gel in the Samco pipette) exceeded three standard deviations of the control's value.

RESULTS

Particle size distribution

For both micelles and nanodroplets, the particle size distribution was bimodal as shown in Figure 3. After the PFP introduction into the solution of micelles, the formation of nanoemulsion was manifested by a disappearance of small micelles (22.2 nm) and generation of nanodroplets (592.6 nm, 73%); a fraction of larger micelles (117.5 nm, 27%) remained in emulsion.

Acoustic droplet vaporization

The goal of these experiments was to examine ultrasound parameters triggering droplet-to-bubble transition in liquid systems and gels.

In the present work, we studied the ADV effect in the block copolymer-stabilized perfluoropentane nanoemulsions that were used in our *in vivo* experiments reported in ref. (Rapoport, Kennedy 2009), except that concentrations of both PFP and block copolymer were increased two-fold in order to increase the sensitivity of subsequent cavitation measurements.

The data obtained for the liquid nanoemulsions may be relevant to the bubble behavior in circulation. However after extravasation into the tumor tissue, the droplets or bubbles are surrounded by a much more viscous extracellular matrix of the tumor interstitium. We modeled this situation by introducing the droplets into a 0.6% agarose gel.

ADV in liquid emulsions

In our experiments, due to density of PFP (1.66 g/cm³), the droplets settled to the bottom of the test tube prior to sonication. The value of the acoustic pressure that induced formation of first visible bubbles that rose from the bottom of the sample was recorded. This pressure

corresponded to or was above the ADV threshold for the formation of primary bubbles (see Methods).

With unfocused ultrasound, bubbles formed a stream that moved upward from the bottom of a container. The volume occupied by the lifted bubbles grew with increased ultrasound intensity. For the majority of particles, the formation of bubbles was reversible and bubbles oscillated up and down, especially under pulsed ultrasound. With significantly increased ultrasound pressure (e.g. 0.61 MPa for CW unfocused ultrasound or between 0.74 and 1.24 MPa for focused ultrasound), some bubbles made it to the sample surface to form foam that comprised large (hundreds of microns) bubbles. These were presumably secondary bubbles that coalesced after vaporization resulting in the formation of stable bubbles with high buoyancy.

ADV in gel matrices

In vivo, after extravasation into tumor tissue, nanodroplets are surrounded by a viscous extracellular matrix where their behavior including response to ultrasound irradiation may be different from that in liquids. To account for the increased viscosity, we introduced nanodroplets in 0.6% agarose gel and monitored nanodroplet vaporization under the action of ultrasound. Studying the ADV effect in gel matrices was complicated by the unavoidable presence of some number of pre-existing large (hundred micron) bubbles that were formed in the process of sample preparation. Low resolution of our 7.5 MHz ultrasound scanner did not allow monitoring in situ formation of small primary microbubbles in gel matrices but post-experiment analysis of ultrasound images using ImageJ software (a public domain image analysis program developed at the National Institutes of Health) allowed discriminating between pre-existing bubbles and newly formed stable microbubbles. The number of the latter, if any, was always very low (one or two per sample) even at the highest negative pressure generated by the unfocused transducer (0.61 MPa at 1 MHz). These results do not however rule out transient and reversible formation of primary microbubbles *via* the ADV in gel matrices. If formed, primary microbubbles are expected to oscillate in ultrasound field thus generating harmonic frequencies, which would confirm their presence. To test this hypothesis, we studied cavitation properties of nanodroplets inserted in liquid emulsions and gels.

Cavitation

In the present study, cavitation effects were explored for unfocused ultrasound and HIFU at a frequency of 1 MHz. The appearance and amplitudes of harmonic frequencies and broadband noise were monitored in the fast Fourier transform emission spectra. Representative frequency spectra are presented in Figure 4. Relative values for second harmonic, subharmonic, and broadband noise amplitudes are presented in Figure 5 A, B for unfocused ultrasound and Figure 6 A, B for HIFU. We need to emphasize that for unfocused ultrasound, the whole volume of the sample (about 300 ml) is sonicated, while less than 5% of the sample is sonicated by HIFU. Therefore for unfocused ultrasound, due to multiple scattering events, the hydrophone collects information from much larger sample volume and “hears” scattered ultrasound at much lower incident ultrasound pressures than those for HIFU. Moreover, measured ADV threshold values depend to high degree on experimental conditions such as sensitivity of a hydrophone, concentration of droplets, ultrasound beam shape, sample volume etc.; therefore threshold values presented in Table 1 are not inherent values for individual droplets. However, for a particular experimental setting, these measurements provide information on the generation of harmonics and broadband noise and allow comparing acoustic properties of various samples. Series (A) of Figures 5 and 6 correspond to liquid emulsions while series (B) correspond to nanodroplets in 0.6% agarose gel. In gel systems, a second harmonic frequency usually appeared at slightly lower pressures than a subharmonic frequency, probably due to lower hydrophone sensitivity at frequencies below 1 MHz (Table 1). The threshold for a subharmonic

frequency component was used as a fingerprint of the onset of stable cavitation, whereas the onset of broadband noise characterized inertial cavitation. The latter can generate shock waves and is considered responsible for cell membrane damage and mechanical cell killing by ultrasound (ter Haar 2004). No broadband noise was observed either for liquid emulsions or gels under unfocused ultrasound, suggesting the absence of inertial cavitation at ultrasound pressures generated by Omnisound 3000 instrument (up to 0.61 MPa). However a second harmonic and subharmonic frequencies were clearly seen in both, liquid emulsions and gels (Figure 5 A, B), with corresponding threshold pressures being slightly lower in gel samples, presumably due to the presence of pre-existing bubbles that catalyze droplet-to-bubble transition (Rapoport, Kennedy 2009, Rapoport, Efros 2009). For the same reason, the pressure dependence of subharmonic amplitude was somewhat smoother for gel samples. The stable cavitation threshold in the gel systems was clearly observed in HIFU experiments, most probably because sonication was confined to small sample volume with low number or absence of pre-existing bubbles (Figure 6 B). Cavitation thresholds were close for both copolymers.

In order to characterize inertial cavitation, we measured mean relative amplitudes of broadband noise in the frequency intervals that avoided fundamental, harmonic, and ultraharmonic frequencies.

As mentioned above, no broadband noise was observed in experiments with unfocused ultrasound while broadband noise was observed in HIFU experiments (Figure 6 E). For HIFU, the thresholds for generating subharmonic frequencies and broadband noise were close suggesting the onset of inertial cavitation (i.e. unstable growth of microbubbles) as soon as the bubbles started oscillating. In contrast, for 1-MHz unfocused ultrasound at ultrasound pressures employed in our *in vivo* studies (Rapoport, Gao 2007; Rapoport, Kennedy 2009), only stable cavitation of microbubbles was observed.

Comparing thresholds for ADV and cavitation in liquid emulsions shows that droplet-to-bubble transition *via* ADV precedes stable and inertial cavitation. The data shown above also indicate that stable microbubble cavitation occurs in both liquid and gel matrices. This suggests that microbubbles are transiently generated and oscillate in gel matrices under the action of unfocused or focused therapeutic ultrasound.

DISCUSSION

Chronologically, this study was completed before the *in vivo* ultrasound-mediated chemotherapy experiments reported in ref. (Rapoport, Kennedy 2009). The data obtained in this study allowed selecting sonication parameters for *in vivo* experiments reported in ref. (Rapoport, Kennedy 2009). Based on the results presented here, unfocused continuous wave 1-MHz ultrasound at a peak rarefactional pressure of 0.61 MPa that reliably induced stable cavitation for both types of droplet-stabilizing copolymers was used *in vivo*. Dramatic regression of ovarian, breast, and pancreatic tumors observed in these experiments suggested that ultrasound-induced stable cavitation of transiently formed microbubbles was sufficient for the efficient drug release and intracellular internalization.

ADV, bubble coalescence, and ultrasound contrast

Nanodroplet vaporization to generate microbubbles is highly desirable for both drug delivery and ultrasonography. Due to large differences in acoustic impedance values for water (1.4 MRayl) and PFP droplets (~0.3 MRayl) or bubbles (\ll 0.3 MRayl), both PFP droplets and bubbles manifest echogenic properties in biological tissues (Kripfgans, Fowlkes 2000); however, bubbles manifest much higher echogenicity than droplets, which creates better contrast in ultrasound images.

Note that only stable bubbles may create sufficient ultrasound contrast in tumor tissue. To our current understanding, the ultrasound-induced formation of stable bubbles proceeds in two steps. Step one is related to droplet-to-bubble transition inside bubble wall that occurs when ADV threshold is reached. In our experiments with liquid emulsions, this event was manifested by the formation of a stream of primary microbubbles directed upward. This primary vaporization event is reversible for droplets whose initial diameter is smaller than 0.8 – 1.2 μm because these droplets generate bubbles with a diameter smaller than 4 – 6 μm for which vaporization temperatures are above 29 °C or physiological temperatures. These primary bubbles condense back into droplets during the ultrasound-off phase of pulsed ultrasound or after termination of sonication. With increased ultrasound intensity, radiation force and microstreaming in liquid matrices accelerate the rate of nanoparticle collisions, which in turn, results in increased rate of coalescence, which is the second step of the formation of stable bubbles. Microbubble condensation and coalescence are competing processes. Increasing ultrasound intensity favors the second process. Because Laplace pressure drops with increasing bubble size, droplet-to-bubbles transition in coalesced droplets or bubbles may become irreversible. These bubbles will be preserved in gaseous phase after termination of sonication. These bubbles generate high ultrasound contrast. The mechanisms described above do not exclude the possibility of preservation of some supercooled primary bubbles after termination of sonication. However, these small bubbles will not produce high ultrasound contrast.

The effects described above are related to bubble behavior in a liquid environment, e.g. in circulation and may be used for Doppler imaging. However, in viscous matrices bubble coalescence was found to be significantly restricted, which resulted in predominantly reversible ultrasound-induced droplet-to-bubble transition. This effect, while sufficient for effective drug delivery, is not adequate for effective ultrasound imaging. Though some formation of stable bubbles was observed in solid tumors sonicated four to five hours after systemic injections of drug-loaded nanoemulsions (data to be reported elsewhere), efficient formation of large stable microbubbles in highly viscous tumor matrices requires higher pressures than those needed for efficient chemotherapy.

Note that microbubble coalescence in the course of sonication results in a shift of particle size distributions towards larger average values, which can result in a change of bubble resonance properties in the course of sonication. Therefore when phase-shift nanoemulsions or microbubbles are used as drug carriers or enhancers of ultrasound-mediated drug delivery, broadband therapeutic transducers appear to be preferable to narrow band transducers.

Cavitation

As discussed above, droplet-to-bubble transition followed by microbubble coalescence is beneficial for contrast-enhanced ultrasound imaging. Even more importantly, only bubbles and not droplets undergo acoustic cavitation, which concentrates ultrasound energy and substantially enhances ultrasound-mediated drug delivery. Though drug delivery from micelles, liposomes, or emulsions may be ultrasonically enhanced even without microbubbles (Dayton, Zhao 2006, Rapoport 2006a, Rapoport 2006b, Rapoport 2007, Rapoport, Marin 2002, Schroeder, Avnir 2007), presence of microbubbles dramatically increased intracellular uptake of drugs or genes (Hernot and Klivanov 2008, Mehier-Humbert, Yan 2007, Rapoport, Gao 2007, Suzuki, Takizawa 2007).

Cavitation is believed to be the main mechanism responsible for ultrasound bioeffects (Chang, Chen 2001, Chen, Brayman 2003, Church and Carstensen 2001, Giesecke and Hynynen 2003, Holland and Apfel 1990, Miller, Averkiou 2008). The oscillation and cavitation of the bubbles triggers release of the encapsulated drug from the carrier and perturbs cell membranes, thus enhancing intracellular drug uptake (Gao, Kennedy 2008, Rapoport, Gao 2007).

The size of our perfluorocarbon nanodroplets (up to 750 nm) allows their localized extravasation through defective tumor microvasculature and accumulation in tumor tissue in vivo. Nanodroplet accumulation in tumor tissue was confirmed by ultrasound imaging (Rapoport, Kennedy 2009). The data for bi-lateral tumors showed that without therapeutic ultrasound, the nanodroplets strongly retained the loaded drug, which resulted in a fast growth of the non-sonicated tumor. On the other hand, the sonicated tumor was dramatically regressed in the course of treatment indicating efficient drug release from the nanocarrier. Strong drug retention in the carrier in the absence of sonication is a positive effect that is important for preventing drug action on non-targeted tissues.

Another advantage of ultrasound-mediated drug delivery in phase-shift nanoemulsions is related to dramatically lower therapeutic ultrasound pressures compared to those used for tumor ablation, which is important in the context of safety of the developed technology.

Strong therapeutic effects (Rapoport, Kennedy 2009) observed in vivo for breast, ovarian, and pancreatic tumors treated with PFP nanoemulsion-encapsulated paclitaxel and unfocused 1-MHz therapeutic ultrasound at 0.61 MPa pressure that did not induce inertial cavitation (see above) suggests that inertial bubble cavitation is not required for efficient drug delivery. The authors of ref. (Datta, Coussios 2008) came to the same conclusion.

Summarizing the results discussed above, combining drug delivery in the phase-shift nanoemulsions with ultrasound-triggered localized drug release may be developed into efficient chemotherapeutic modality for solid tumors.

Acknowledgments

The project described was supported by Grant Number R56EB001033 and R01EB001033 to NR from the National Institute Of Biomedical Imaging And Bioengineering. The content is solely the responsibility of the authors and does not necessarily represent the official views of the National Institute Of Biomedical Imaging And Bioengineering or the National Institutes of Health. The authors are grateful to Dr. A. Efros for productive discussions.

REFERENCES

- Barber EJ, Cady GH. Vapor pressures of perfluoropentanes. *J Phys Chem* 1956;60:504–05.
- Bekeredjian R, Chen S, Frenkel PA, Grayburn PA, Shohet RV. Ultrasound-targeted microbubble destruction can repeatedly direct highly specific plasmid expression to the heart. *Circulation* 2003;108:1022–6. [PubMed: 12912823]
- Campbell RB. Tumor physiology and delivery of nanopharmaceuticals. *Anticancer Agents Med Chem* 2006;6:503–12. [PubMed: 17100555]
- Chang PP, Chen WS, Mourad PD, Poliachik SL, Crum LA. Thresholds for inertial cavitation in albumin suspensions under pulsed ultrasound conditions. *IEEE Trans Ultrason Ferroelectr Freq Control* 2001;48:161–70. [PubMed: 11367783]
- Chappell JC, Klibanov AL, Price RJ. Ultrasound-microbubble-induced neovascularization in mouse skeletal muscle. *Ultrasound Med Biol* 2005;31:1411–22. [PubMed: 16223645]
- Chen WS, Brayman AA, Matula TJ, Crum LA. Inertial cavitation dose and hemolysis produced in vitro with or without Optison. *Ultrasound Med Biol* 2003;29:725–37. [PubMed: 12754072]
- Church CC, Carstensen EL. “Stable” inertial cavitation. *Ultrasound Med Biol* 2001;27:1435–7. [PubMed: 11731057]
- Clasohm LY, Vakarelski IU, Dagastine RR, Chan DY, Stevens GW, Grieser F. Anomalous pH dependent stability behavior of surfactant-free nonpolar oil drops in aqueous electrolyte solutions. *Langmuir* 2007;23:9335–40. [PubMed: 17665938]
- Datta S, Coussios CC, Ammi AY, Mast TD, de Courten-Myers GM, Holland CK. Ultrasound-enhanced thrombolysis using Definity as a cavitation nucleation agent. *Ultrasound Med Biol* 2008;34:1421–33. [PubMed: 18378380]

- Dayton PA, Zhao S, Bloch SH, Schumann P, Penrose K, Matsunaga TO, Zutshi R, Doinikov A, Ferrara KW. Application of ultrasound to selectively localize nanodroplets for targeted imaging and therapy. *Mol Imaging* 2006;5:160–74. [PubMed: 16954031]
- Ferrara K, Pollard R, Borden M. Ultrasound microbubble contrast agents: fundamentals and application to gene and drug delivery. *Annu Rev Biomed Eng* 2007;9:415–47. [PubMed: 17651012]
- Ferrara KW. Driving delivery vehicles with ultrasound. *Adv Drug Deliv Rev* 2008;60:1097–102. [PubMed: 18479775]
- Ferrara K, Borden M, Zhang H. Lipid-Shelled Vehicles: Engineering for Ultrasound Molecular Imaging and Drug Delivery. *Acc. Chem. Res.* 2009 PMID: 19552457.
- Gao Z, Kennedy AM, Christensen DA, Rapoport NY. Drug-loaded nano/microbubbles for combining ultrasonography and targeted chemotherapy. *Ultrasonics* 2008;48:260–70. [PubMed: 18096196]
- Giesecke T, Hynynen K. Ultrasound-mediated cavitation thresholds of liquid perfluorocarbon droplets in vitro. *Ultrasound Med Biol* 2003;29:1359–65. [PubMed: 14553814]
- Greenleaf WJ, Bolander ME, Sarkar G, Goldring MB, Greenleaf JF. Artificial cavitation nuclei significantly enhance acoustically induced cell transfection. *Ultrasound Med Biol* 1998;24:587–95. [PubMed: 9651968]
- Hernot S, Klivanov AL. Microbubbles in ultrasound-triggered drug and gene delivery. *Adv Drug Deliv Rev* 2008;60:1153–66. [PubMed: 18486268]
- Hobbs SK, Monsky WL, Yuan F, Roberts WG, Griffith L, Torchilin VP, Jain RK. Regulation of transport pathways in tumor vessels: role of tumor type and microenvironment. *Proc Natl Acad Sci U S A* 1998;95:4607–12. [PubMed: 9539785]
- Holland CK, Apfel RE. Thresholds for transient cavitation produced by pulsed ultrasound in a controlled nuclei environment. *J Acoust Soc Am* 1990;88:2059–69. [PubMed: 2269722]
- Hynynen K. Ultrasound for drug and gene delivery to the brain. *Adv Drug Deliv Rev* 2008;60:1209–17. [PubMed: 18486271]
- Iyer AK, Khaled G, Fang J, Maeda H. Exploiting the enhanced permeability and retention effect for tumor targeting. *Drug Discov Today* 2006;11:812–8. [PubMed: 16935749]
- Kinoshita M, McDannold N, Jolesz FA, Hynynen K. Noninvasive localized delivery of Herceptin to the mouse brain by MRI-guided focused ultrasound-induced blood-brain barrier disruption. *Proc Natl Acad Sci U S A* 2006;103:11719–23. [PubMed: 16868082]
- Kripfgans OD, Fabiilli ML, Carson PL, Fowlkes JB. On the acoustic vaporization of micrometer-sized droplets. *J Acoust Soc Am* 2004;116:272–81. [PubMed: 15295987]
- Kripfgans OD, Fowlkes JB, Miller DL, Eldevik OP, Carson PL. Acoustic droplet vaporization for therapeutic and diagnostic applications. *Ultrasound Med Biol* 2000;26:1177–89. [PubMed: 11053753]
- Lo AH, Kripfgans OD, Carson PL, Rothman ED, Fowlkes JB. Acoustic droplet vaporization threshold: effects of pulse duration and contrast agent. *IEEE Trans Ultrason Ferroelectr Freq Control* 2007;54:933–46. [PubMed: 17523558]
- Mehier-Humbert S, Yan F, Frinking P, Schneider M, Guy RH, Bettinger T. Ultrasound-mediated gene delivery: influence of contrast agent on transfection. *Bioconjug Chem* 2007;18:652–62. [PubMed: 17419583]
- Miller DL, Averkiou MA, Brayman AA, Everbach EC, Holland CK, Wible JH Jr, Wu J. Bioeffects considerations for diagnostic ultrasound contrast agents. *J Ultrasound Med* 2008;27:611–32. quiz 33–6. [PubMed: 18359911]
- Miller DL, Gies RA. The interaction of ultrasonic heating and cavitation in vascular bioeffects on mouse intestine. *Ultrasound Med Biol* 1998;24:123–8. [PubMed: 9483779]
- Rapoport, N. Combined cancer therapy by micellar-encapsulated drug and ultrasound. In: Amiji, M., editor. *Nanotechnology for cancer therapy*. CRC Press; Boca Raton (FL): 2006a. p. 417-37.
- Rapoport, N. Tumor targeting by polymeric assemblies and ultrasound activation. In: Arshadi, R.; Kono, K., editors. *MML*. Kentus Books; London (UK): 2006b. p. 305-62.
- Rapoport N. Physical stimuli-responsive polymeric micelles for anti-cancer drug delivery. *Prog Polym Sci* 2007;32:962–90.

- Rapoport N, Gao Z, Kennedy A. Multifunctional nanoparticles for combining ultrasonic tumor imaging and targeted chemotherapy. *J Natl Cancer Inst* 2007;99:1095–106. [PubMed: 17623798]
- Rapoport N, Kennedy AM, Shea JE, Scaife CL, Nam KH. Controlled and targeted tumor chemotherapy by ultrasound-activated nanoemulsions/microbubbles. *J Control Release*. 2009 In press (doi:10.1016/j.jconrel.2009.05.026).
- Rapoport N, Marin A, Christensen DA. Ultrasound-activated micellar drug delivery. *Drug Delivery Syst Sci* 2002;2:37–46.
- Rapoport NY, Efros AL, Christensen DA, Kennedy AM, Nam KH. Microbubble generation in phase-shift nanoemulsions used as anticancer drug carriers. *Bub Sci Eng Tech* 2009;1:31–39.
- Schroeder A, Avnir Y, Weisman S, Najajreh Y, Gabizon A, Talmon Y, Kost J, Barenholz Y. Controlling liposomal drug release with low frequency ultrasound: mechanism and feasibility. *Langmuir* 2007;23:4019–25. [PubMed: 17319706]
- Skyba DM, Price RJ, Linka AZ, Skalak TC, Kaul S. Direct in vivo visualization of intravascular destruction of microbubbles by ultrasound and its local effects on tissue. *Circulation* 1998;98:290–3. [PubMed: 9711932]
- Stieger SM, Caskey CF, Adamson RH, Qin S, Curry FR, Wisner ER, Ferrara KW. Enhancement of vascular permeability with low-frequency contrast-enhanced ultrasound in the chorioallantoic membrane model. *Radiology* 2007;243:112–21. [PubMed: 17392250]
- Suzuki R, Takizawa T, Negishi Y, Haggisawa K, Tanaka K, Sawamura K, Utoguchi N, Nishioka T, Maruyama K. Gene delivery by combination of novel liposomal bubbles with perfluoropropane and ultrasound. *J Control Release* 2007;117:130–6. [PubMed: 17113176]
- ter Haar, GR. *Ultrasonic biophysics*. Wiley; Chichester (UK): 2004.
- Unger EC, Porter T, Culp W, Labell R, Matsunaga T, Zutshi R. Therapeutic applications of lipid-coated microbubbles. *Adv Drug Deliv Rev* 2004;56:1291–314. [PubMed: 15109770]
- Wheatley MA, Forsberg F, Oum K, Ro R, El-Sherif D. Comparison of in vitro and in vivo acoustic response of a novel 50:50 PLGA contrast agent. *Ultrasonics* 2006;44:360–7. [PubMed: 16730047]

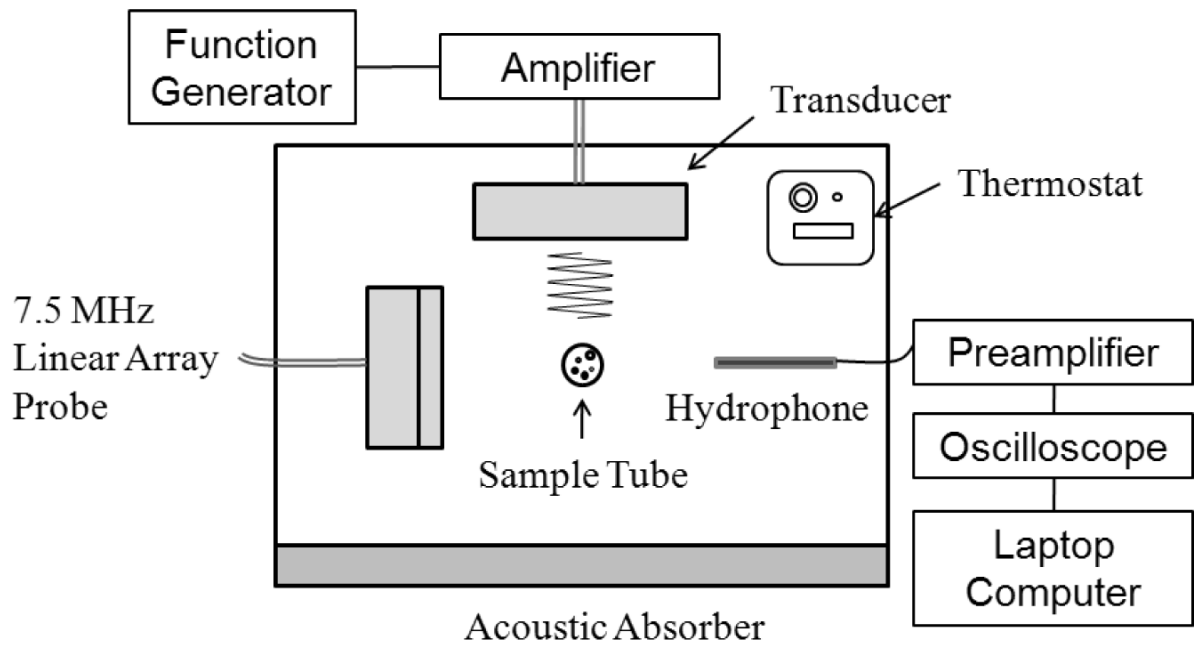


Figure 1A. Schematic representation of the top view of experimental setup used for monitoring acoustic droplet vaporization or cavitation.

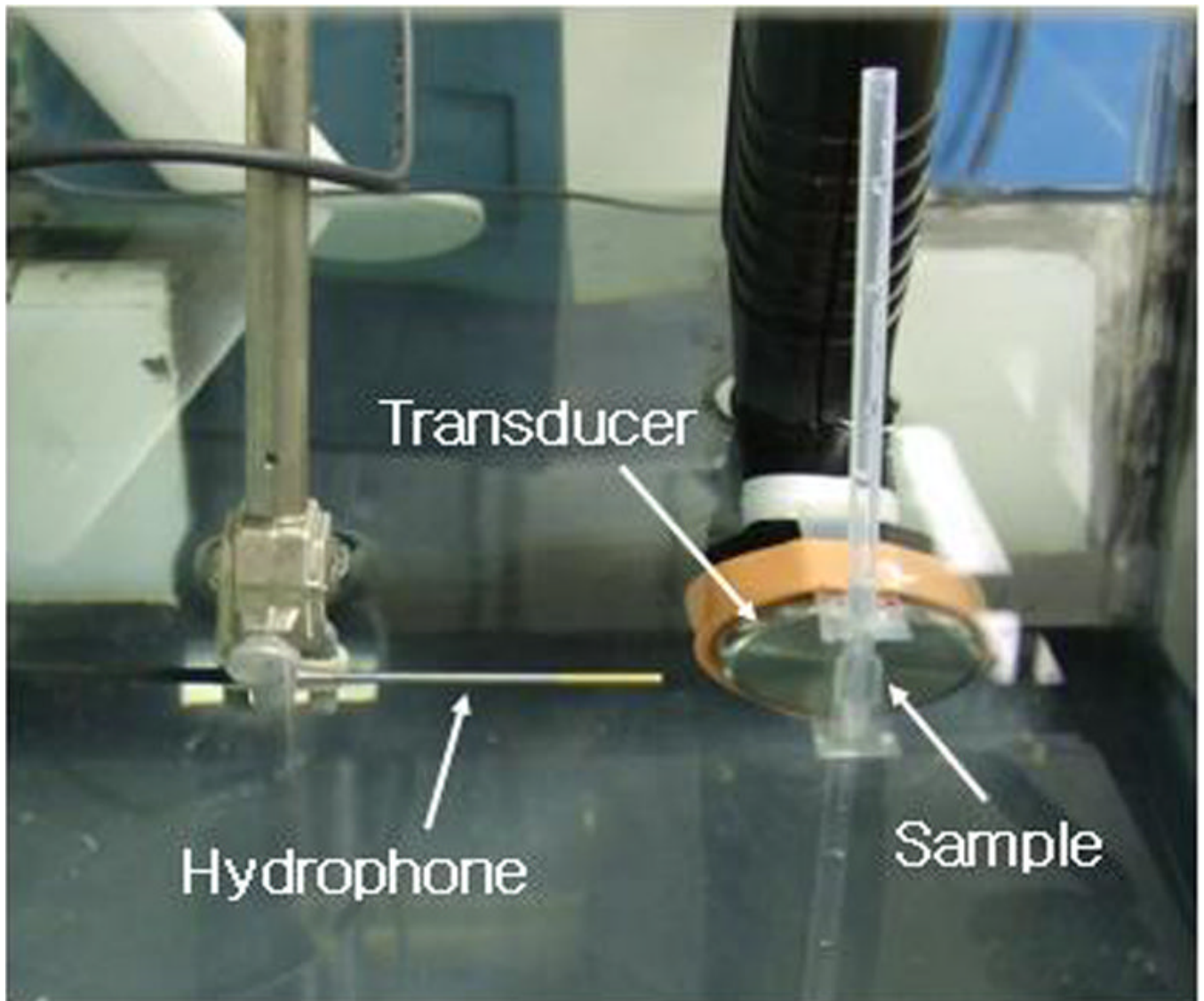


Figure 1B. The top view of the experimental set used for measurements of the acoustic properties of nanodroplets/microbubbles; details in the text.

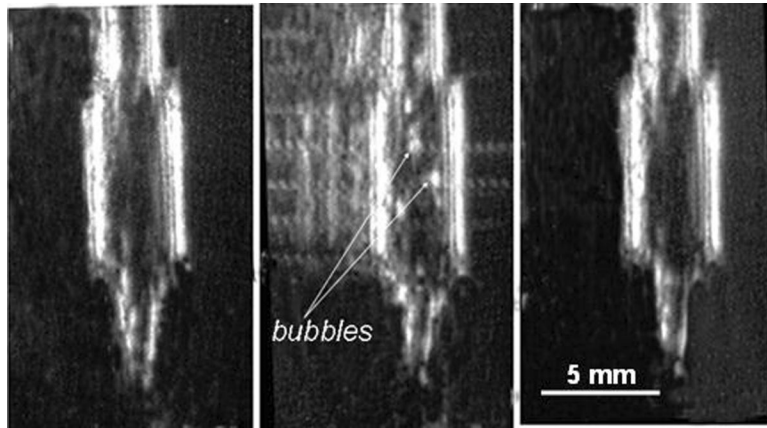


Figure 2.

An example of ultrasound images used to monitor ADV effects; a test tube with PEG-PCL nanoemulsion is shown (a) - before sonication; (b) - during sonication by unfocused CW 1-MHz ultrasound at a pressure of 0.61 MPa; (c) - after termination of sonication. Reverberations were artificially removed to clarify the images.

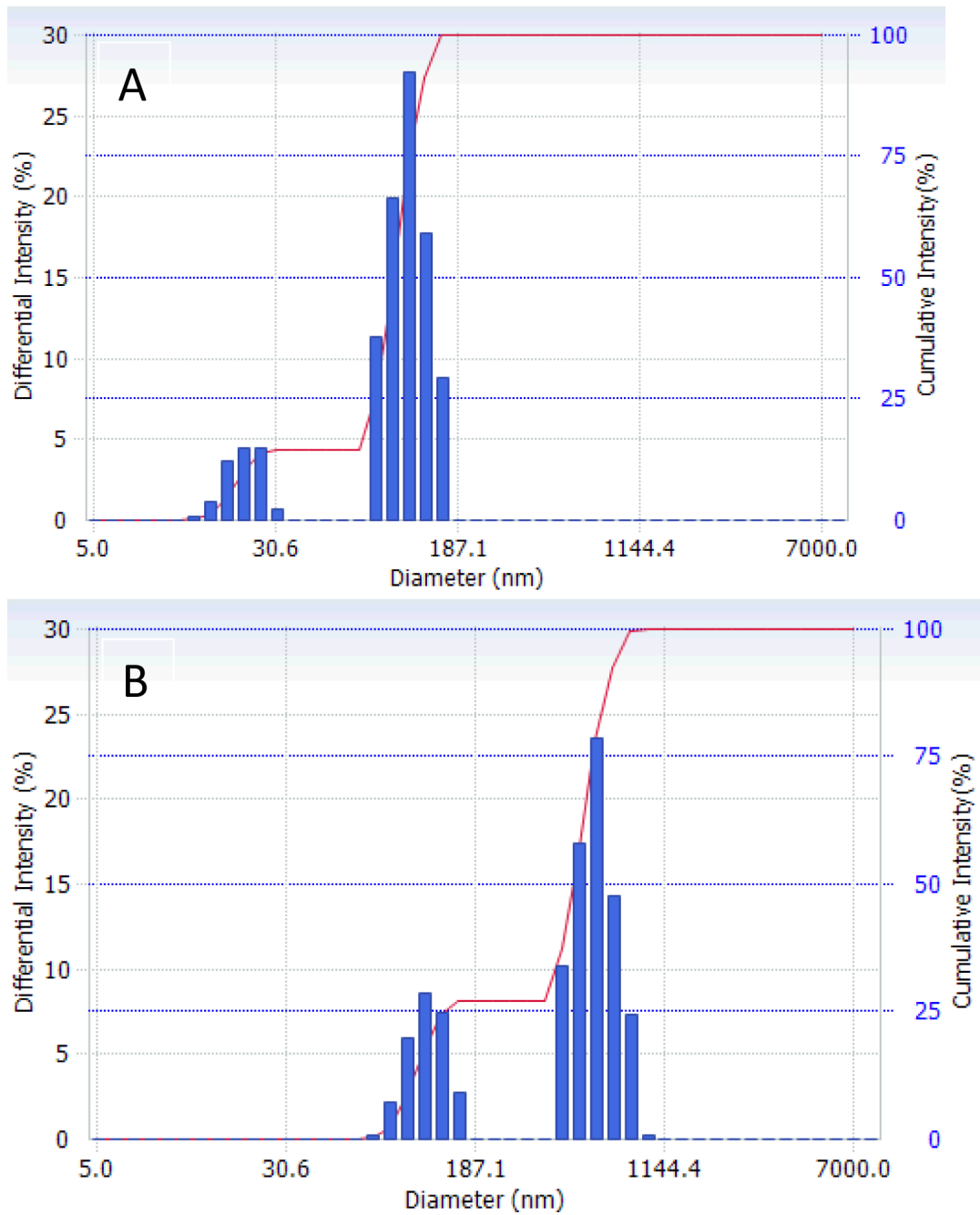


Figure 3. Particle size distribution in (a) 0.25 % PEG-PLLA micelles; (b) 2 % PFP/0.5 % PEG-PLLA nanodroplets.

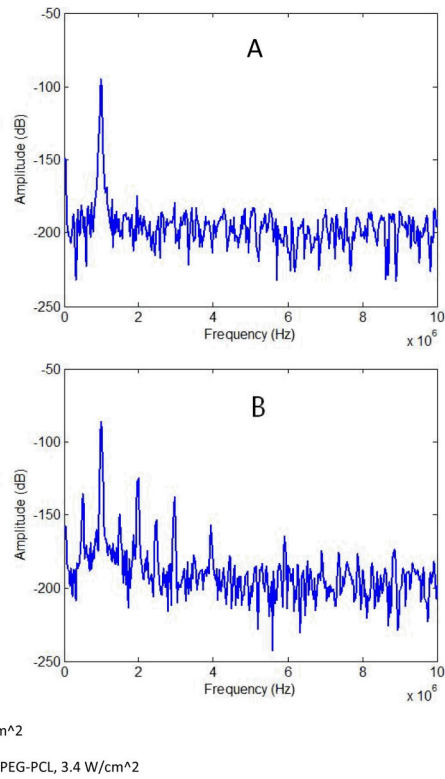


Figure 4. Representative frequency spectra for (a) - water in a tank sonicated by unfocused 1-MHz ultrasound at a pressure of 0.27 MPa; and (b) - 1% PFP/0.25% PEG-PCL nanoemulsion in a test tube sonicated by unfocused 1-MHz ultrasound at a pressure of 0.61 MPa.

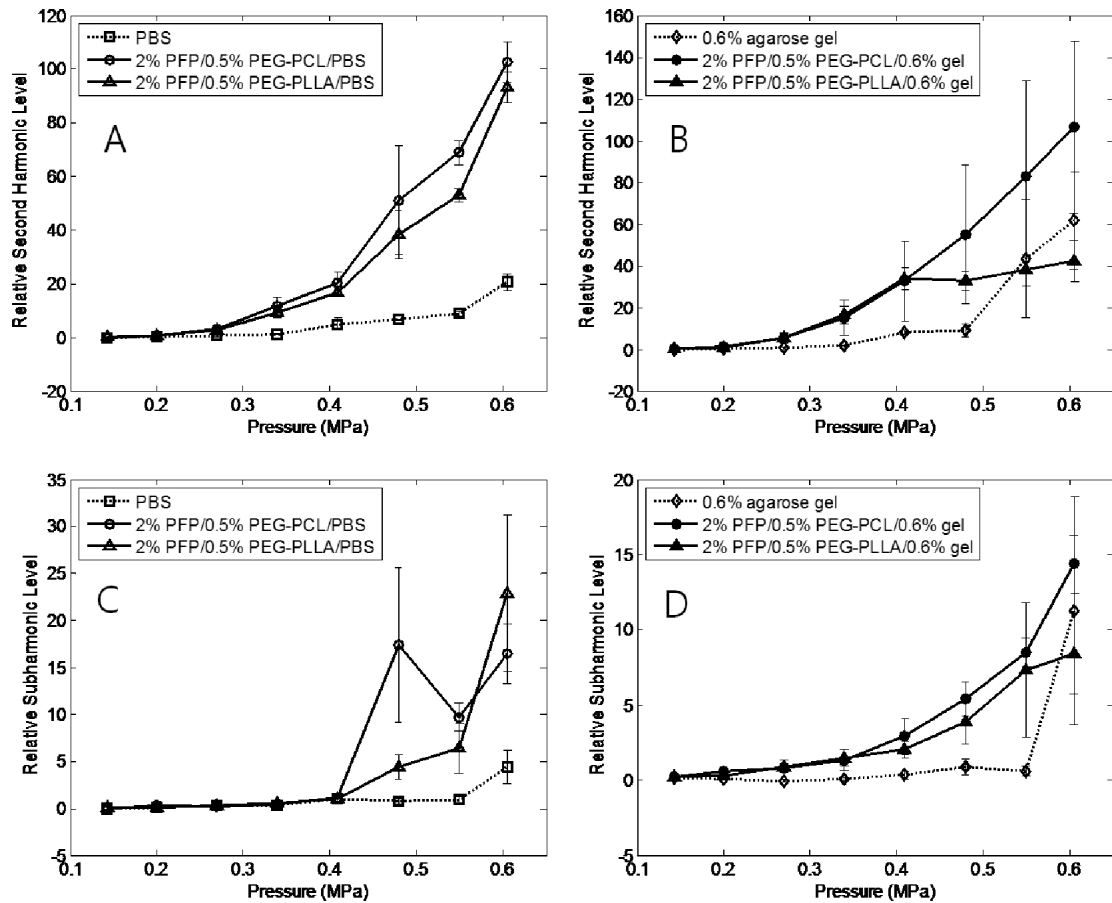


Figure 5. Stable cavitations as characterized by relative second harmonic (A, B) or subharmonic (C,D) amplitudes generated by the microbubbles in PBS (A, C) or agarose gel (B, D); the fundamental frequency is 1 MHz.

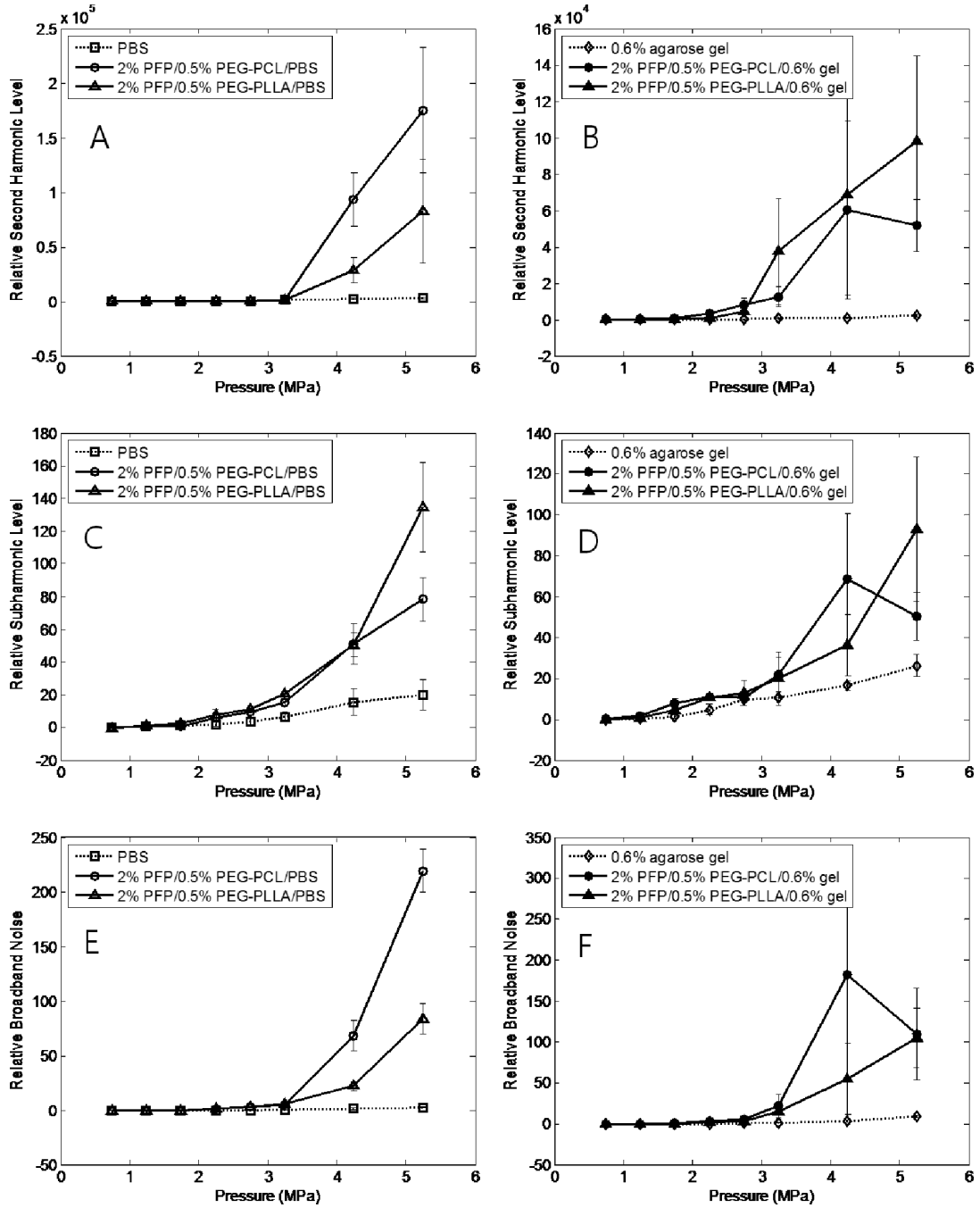


Figure 6. Stable (A, B, C, D) and inertial (E,F) cavitation as characterized by relative second harmonic subharmonic (A, B), subharmonic (C,D) or broadband noise (E,F) amplitudes generated by the microbubbles in PBS (A, C, E) or agarose gel (B, D, F) under HIFU ultrasound; the fundamental frequency is 1 MHz.

Table 1

Acoustic parameters of nanodroplets in liquid emulsions or 0.6% agarose gels.

Ultrasound	Frequency component	Threshold, MPa*			
		2% PFP 0.5% PEG-PCL		2% PFP 0.5% PEG-PLLA	
		PBS	GEL	PBS	GEL
1 MHz HIFU	Second harmonic	3.2 – 4.2	2.7 – 3.2	3.2 – 4.2	2.7 – 3.2
	Subharmonic	3.2 – 4.2	3.2 – 4.2	3.2 – 4.2	3.2 – 4.2
	Broadband noise	3.2 – 4.2	3.2 – 4.2	3.2 – 4.2	3.2 – 4.2
1 MHz unfocused	Second harmonic	0.41 – 0.48	0.30 – 0.34	0.41 – 0.48	0.30 – 0.34
	Subharmonic	0.41 – 0.48	0.34 – 0.41	0.41 – 0.48	0.34 – 0.41
	Broadband noise	>0.61	>0.61	>0.61	>0.61

* Due to a stepwise increase of ultrasound intensity, the data are presented as a range between the pressure that is below threshold and the next step pressure that is above threshold.